An Investigation of the Impact of Forming Process Parameters in Single Point Incremental Forming Using Experimental and Numerical Verification

Marwan T. Mezher[1]*, Béla Kovács[2]

[1] Department of Jewelry Art Techniques, Institute of Applied Arts, Middle Technical University, Baghdad 10074, Iraq
[2] Department of Analysis, Institute of Mathematics, Faculty of Mechanical Engineering and Informatics, University of Miskolc, Miskolc-Egyetemváros, 3515 Miskolc, Hungary
* Corresponding author, e-mail: marwantahir90@mtu.edu.iq

Abstract

Incremental sheet forming (ISF) is an innovative cold forming operation and has enticed great interests owing to its flexibility and capability to manufacture various complex 3D shapes with low costs and minimum requirements. Single point incremental forming (SPIF) is the most popular type of ISF process and has high quality and less occurrence of defects for the formed products if the operating parameters are achieved and evaluated with high precision. In this study, the impact of tool diameter and forming angle on the forming force, thickness distribution, thinning ratio, effective plastic strain, forming depth and fracture behaviour was explored. AA1050 aluminium alloy and DC04 carbon steel were employed to produce a truncated cone in accordance with the SPIF process. A 3D finite element model was required to achieve a well-established investigation. The SPIF of a truncated cone numerical model was adopted to build a model with the same conditions as of the experimental work with aid of ANSYS software version 18 through using the workbench LS-DYNA model. The sheet metal modelling was carried out in accordance the Cowper Symonds power law hardening by taking the behaviour of the material as elastic–plastic, and the anisotropic properties were assumed to simulate the plasticity behaviour for two sheet metals. Results indicate that the DC04 carbon steel has a higher forming force, minimum thickness and lower thinning ratio compared with AA1050 aluminium alloy under the same operating conditions.

Keywords

SPIF, forming force, ANSYS, thickness distribution, thinning ratio, effective plastic strain

1 Introduction

The incremental sheet forming (ISF) process is distinguished with small mass production, low cost and high customisation [1, 2], and it is accomplished with the accumulation of the plastic deformation for the sheet material, in which a spherical forming tool is controlled through a computer programme to produce various complex shapes of the sheet metals [3, 4]. The single point incremental forming (SPIF) process is receiving greater research attention amongst the various modes of ISF due to its minimum experimental requirements to produce the desired shape [5].

In contrast with the conventional sheet metal forming operations, such as deep drawing and stamping, which need to have dedicated forming tools and dies, this unconventional ISF process reduces the cost by avoiding the using special dies and forming tools [6]. When the sheet metal is squeezed and deformed locally by the tool, the

forming force becomes a crucial factor concerning the failure mechanism and accuracy of the manufactured parts. Forming leads to strain and stress in the blank material relying upon the formed component shape, which further decided the structural integrity of the final product [7].

Various numerical and experimental studies have emphasized the investigation of forming loads generated during the SPIF operation, the thickness distribution of the wall profile and the influence of different operating parameters. Aerens et al. [8] investigated the impact of tool diameter and wall angle on the forming force of AA3003. The results exhibited that the axial forming force was higher than the tangential forming force, and the increase in profile angle and tool diameter resulted in an increase in the forming force. Duflou et al. [9, 10] noted similar observations of forming force trends for AA3103-O with

different forming tool diameters. Bagudanch et al. [7] analysed the influence of tool diameter on the forming force of AISI304 stainless steel through SPIF operation. The findings revealed that the forming force raised with the increase in the tool diameter. Filice et al. [11] carried out a group of tests on AA1050-O. The results showed that maximum tangential force increased due to the increase in the wall angle, and three types of forming force trends were observed. Kumar et al. [12] studied the effect of forming angle and tool diameter on AA2024-O through the ISF operation. The results indicated that the resultant forming force intensified with the increase in wall angle and tool diameter. Kumar and Gulati [13] also noticed that the maximum axial force remarkably increased with the increase in the wall angle and tool diameter of AA6063 and AA2024-O sheet metals through the ISF operation.

Pohlak et al. [14] investigated the forming force through the SPIF operation using numerical and experimental investigation. They found that the numerical resultant force was consistent with the experimental ones. Li et al. [15] developed a finite element model employing LS-Dyna software of AA7075-O. The results revealed that the experimental forming force were slightly smaller than the predicated horizontal and vertical forces. Li et al. [16, 17] predicated the tangential forming force by employing LS-DYNA software in the SPIF operation. Fiorentino [18] suggested a failure criterion relying upon the observation of forming forces trend throughout the forming operation. This approach was built by comparing the ultimate tensile strength of the sheet material and stresses value that acting on the sheet material. Lu et al. [19] noticed that the friction force during the SPIF process was reduced by replacing the traditional rigid forming tool with a roller ball type tool. Neto et al. [20] evaluated the generated strain and wall thickness of AA7075-O aluminium alloy through the SPIF operation. They concluded that the final formed part thickness is decreased with increasing wall angle. Furthermore, the plastic strain was symmetrically distributed for the cone formed part, and the generated plastic strain on the inner surface was more on the outer side. Emmens et al. [21] proposed that the predominant deformation mechanisms in the SPIF process are hydrostatic pressure, bending, cyclic straining and shear.

Jackson and Allwood [22] observed deformation mechanism experimentally during the SPIF process composed mainly of stretching deformation perpendicular to the tool path and through the thickness shear along and perpendicular to the movement of the tool path. They noticed

the shear raised when the deformation depth increased. Ambrogio et al. [23] carried out an experimental study on AA1050-O and noticed that the forming force gradually raised up to a maximum value as a result of the bending mechanism of the sheet material; then, it commenced to reduce up to a certain value. Oraon and Sharma [24] estimated the surface quality of formed products during the SPIF process by developing the artificial neural network model. They stated a result of 94.744% for the neural network model performance with an average error of 1.068%. Petek et al. [25] reported that the combination between higher wall angle and larger tool diameter showed a higher forming force. Blaga et al. [26] and Filice et al. [11] noted that the interaction between the larger step size and forming tool diameter increased the resultant forming force. Abdelkader et al. [27] adopted numerical and experimental investigation to analyse the impact of wall angle on the thickness distribution of a truncated cone throughout the SPIF technique. They reported that the minimum thickness decreased with the increase in the forming angle. The thinning ratio was noticed at the 65° wall angle twice times greater compared with 45°.

Arfa et al. [28] inferred that the thickness greatly decreased with the increase in the wall angle of the truncated cone. The results showed that the final thickness in the wall profile significantly decreased from 1.2 mm (initial thickness) to 0.649, 0.524 and 0.440 mm for the 55°, 60° and 65° wall angle, respectively. Mezher et al. [29] investigated the impact of the nanoparticle additives of AA2024-T4 through the SPIF process. They pointed out that the quality of the formed parts significantly improved when nanoparticle additives were used. Namer et al. [30] showed that the SPIF process parameters of the polymer sheets remarkably enhanced when the lubricant viscosity increased. Li et al. [31] experimentally and numerically analysed the influence of tool diameter on the forming depth, minimum thickness and plastic strain of the formed components during the SPIF operation. They found that the increase in tool diameter results in the increase in forming depth and minimum thickness, whilst the plastic strain was decreased when a larger tool diameter was used. Golabi et al. [32] observed the same finding regarding the formability. Mezher et al. [33] studied the effect of pre-cut holes, minimum thickness, thinning ratio, plastic strain and forming force by using a hole flanging process with the aid of SPIF. They found that the forming force and plastic strain were higher when a smaller initial diameter and plastic strain were used, and the thickness

distribution curve was enhanced with larger pre-cut holes. Other researchers studied the SPIF process using aluminium foils with a 0.22 initial thickness to investigate the impact of hemispherical and flat forming tools. They observed that the formability and formed component accuracy were significantly enhanced when a flat-end tool was used [34, 35]. Najm et al. [36, 37] analysed the influence of tool diameter, feed rate, tool speed and lubricant type on the resultant hardness of the formed components of AA1100. The findings indicate that a higher feed rate and tool speed enhanced the hardness whilst increasing the tool diameter, resulting in the reduction of hardness. The hardness was increased when coolant oil was used, and the effect on hardness was opposite when grease was used as a lubricant. Two papers have analysed the impact of tool characteristics on the quality of formed parts by using an Artificial Neural Network and Support Vector Regression. The authors developed regression equations to numerically predict the surface roughness [38, 39].

The analysis of the above literature reviews showed that the effect of wall angle and tool diameter on the forming force, thickness distribution and thinning ratio is complex. Investigating the maximum forming force, final minimum thickness and thinning consider a big issue of a truncated cone during the SPIF process. Good interaction amongst these parameters might have a direct impact on producing high-quality formed components. On this basis, this work attempted to address these issues. A truncated cone was manufactured from two sheet metals, namely, AA1050 aluminium alloy and DC04 carbon steel employing the SPIF operation, to analyse the effect of wall angles and tool diameters on the forming force evolution, thickness distribution, thinning ratio, effective plastic strain and fracture behaviour. Five different tool diameters (8, 10, 12, 14, and 16 mm) and forming angles (45°, 55°, 65°, 70°, 72° and 75°) were used. The generated friction between the forming tool contact and the sheet surface was decreased by employing hybrid nano-lubricant additives based on the observations reported by Namer et al. [40].

2 Methodology and experimental procedures
2.1 SPIF process
Square blanks of AA1050 aluminium alloy and DC04 carbon steel with dimensions of (200 × 200 × 1 mm) were employed to perform the experiments during the SPIF process. A series of SPIF tests was experienced on a three-axis milling CNC machine TX32, as shown in Fig. 1.

The SPIF setup consists of a backing plate with 100 mm as a diameter hole, and a blank holder, and they are fixed to the table of the CNC milling machine by a rigid rig. The forming tool was fixed to the CNC machine's vertical part. The sheet metals were mounted and fixed over the backing plate and incrementally deformed by using the spherical forming tool according to a specified forming path. The tool path was computerised by using G-code language to control the tool movement in the Z direction following a spiral conical path with changing slope in each experiment to obtain a different angle. The helical path is determined by successive linear interpolations as permitted by the precision of the CNC milling control, and a step-down equal to 0.05 mm per revolution was selected in all helical path steps. The other working conditions, such as feed rate and spindle speed were set to equal 600 mm/min and 450 rev/min, respectively. Fig. 2 depicts some formed components.
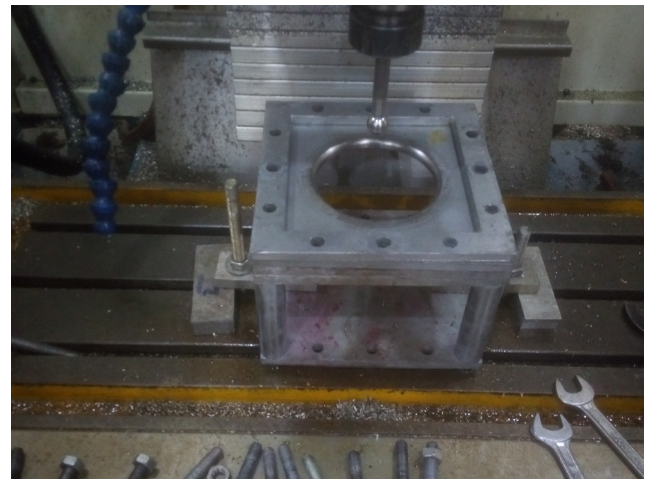

Fig. 1 SPIF tools on the CNC milling machine

Fig. 2 Specimens of truncated cones

2.2 Material properties

The investigated sheet metals in this research are DC04 carbon steel and AA1050 aluminium alloy with 1 mm thickness. The mechanical properties are determined by employing a set of tensile tests using a hydraulic press with a peak loading power equal to 30 tons. The dimensions of the tensile specimen were taken according to ASTM-E8/E8M-21 standard [41], and the mechanical properties are summarised in Table 1.

3 Simulation of the SPIF process

According to the literature review, the numerical modelling of the SPIF process is a powerful tool to predict the results before commencing the experimental work. The advantages of utilising modelling and simulation programmes prior to trying new experiments are minimising the total time required for the experimental procedures, increasing the performance and reducing the errors. Moreover, simulation software, such as ANSYS, is a vital method for the optimisation of the SPIF process parameters.

Finite element simulation through the SPIF operation considers a time-consuming and complex process due a number of nonlinearities and larger tool trajectories [42]. These very long trajectories can be solved by employing time scaling and mass scaling methods in the explicit solver, reducing the computing time required to solve the SPIF process.

To assess the influence of the wall angles and tool diameters on the quality of the manufactured parts of AA1050 aluminium alloy and DC04 carbon steel throughout the SPIF process, a 3D finite element model was established by using a commercial finite element software ANSYS version 18 (workbench LS-DYNA model) to build the 3D model. Meanwhile, the evaluation of the outcomes was achieved by using LS-PREPOST software. The SPIF FE model was parameterised to create a truncated cone, such as the experimental work with different forming angles. The results such as forming force, thickness distribution, thinning ratio, effective plastic strain and fracture behaviour, were analysed during the numerical investigation.

Table 1 Mechanical properties of blank materials

Properties	AA1050	DC04
Tensile strength (MPa)	152	335
Yield strength (MPa)	33	215
Strength coefficient (K) (MPa)	218	510
Hardening exponent (n)	0.23	0.21
Poisson's ratio (n)	0.33	0.3
Young modulus (GPa)	69	210

An elastic–plastic behaviour was assumed to model the sheet metal, and the elastic properties were modelled based on Poisson's ratio and Young modulus, as depicted in Table 1. The tools (backing and clamping plates) were modelled as rigid fixed bodies. The forming tool was simulated as a rigid translating body, whereas the workpiece material was defined as a deformable body. Based on the findings for creating the simulation of forming operations in [43, 44], a Cowper–Symonds anisotropic yielding criterion was implemented to model the plasticity behaviour of the sheet material with the same mechanical properties that are shown in Table 1. A fully integrated shell element formulation was used to mesh and discretise the sheet material with seven integration points throughout the sheet thickness, and the element size was set to 0.002 mm.

A surface to surface forming formulation was employed to simulate the contact interface between the SPIF parts (forming tool–sheet material, sheet material–backing plate and clamping plate–sheet material) with soft constraint formulation. In terms of the contact conditions, Coulomb's friction law with a coefficient of friction set to 0.0331 was employed for the hybrid nanoparticles (CuO and MoS_2) that were added to sunflower oil based on the findings by Namer et al. [40]. Meanwhile, the simulation running time was reduced by using a proper mass scaling factor of 1000, in which the ratio of the kinetic energy to the internal energy remained below 1%. Furthermore, Flanagan–Belytschko stiffness form was used to apply the hourglass control to decrease the integration. Fig. 3 shows the SPIF meshed model.
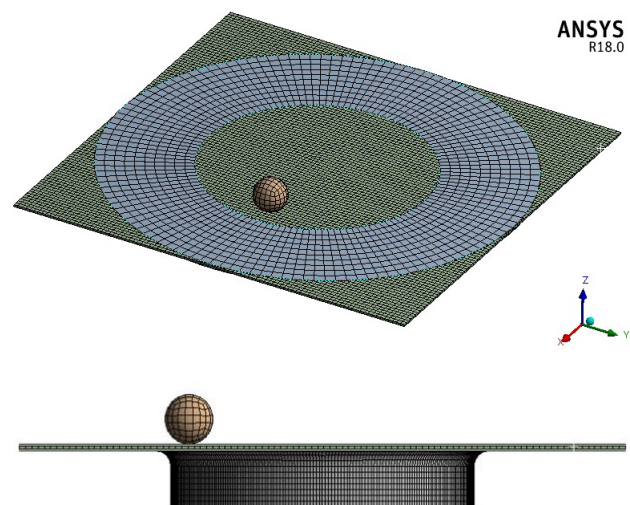

Fig. 3 SPIF numerical model

4 Results and discussions

4.1 Effect of tool diameter

Sorting and determining the optimal tool diameter are necessary. Consequently, preliminary tests were conducted to identify the influence of forming tool diameters on the resultant force, minimum thickness, maximum thinning ratio, forming depth (formability) and effective plastic strain. Five different incremental forming tools with varying diameters (8, 10, 12, 14, and 16 mm) were used to form a truncated cone from the AA1050 aluminium alloy as a preliminary experiment. When the sheet metal is locally deformed by the forming tool, the resultant forming force has an influence on the fracture mode and formed component quality because the forming forces create strains and stresses that determine the structural integrity of the formed components. The amplitude of the predicated forming force through the SPIF numerical model gradually increases from the start of the operation to the maximum value with the increase in tool diameter as a result of the greater contact region between the tool and the blank interface, and more metal is formed during this stage, which are consistent with results in [7–10] and [12]. Meanwhile, the running time for a larger tool diameter decreases compared with utilising a smaller tool diameter due to the use of a larger step size.

In Fig. 4, the numerical findings of the forming force of the diameters (8 and 10 mm) reveal an instability in the curve of the forming force. This up and down trend demonstrates severe thinning in some regions of the formed components, resulting in zones of risk of cracks in comparison with diameters (12, 14 and 16 mm). This phenomenon occurs because the curved surface contact area, which is in direct contact with the surface of the sheet metal, will be small when a small tool diameter is used, resulting in more penetration in the sheet metal. Furthermore, the large curved surface area of the bigger tool diameter results in
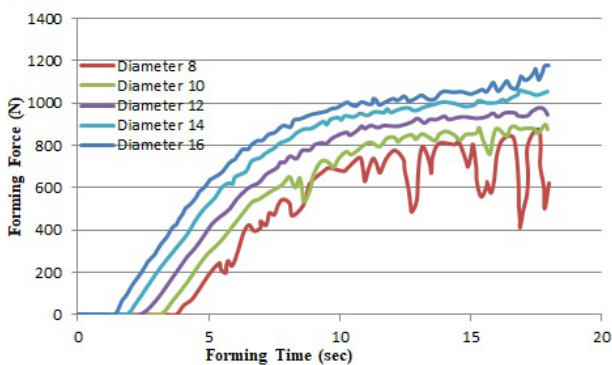
more smoothing of the sheet surface compared with the small curved surface area as shown Fig. 5, which depicts the key of formability for the different tool diameters.

Fig. 6 exhibits the impact of forming tool diameter on the minimum thickness and thinning ratio. The results indicate that the minimum thickness and thinning ratio have an inverse relationship with forming tool diameter. This notion means that the larger tool diameter gives bigger minimum thickness and lower thinning ratio due to the same aforementioned reasons for the influence of tool diameter on the forming force, which are consistent with the results in [31].

Fig. 7 shows another interesting observation of the influence of tool diameter on the final forming depth. The findings show that the forming depth increased from nearly 25.35 mm at 8 mm tool diameter to 29.39 mm at 16 mm tool diameter. These findings indicate the formability of truncated cone enhanced by 13.69% when using
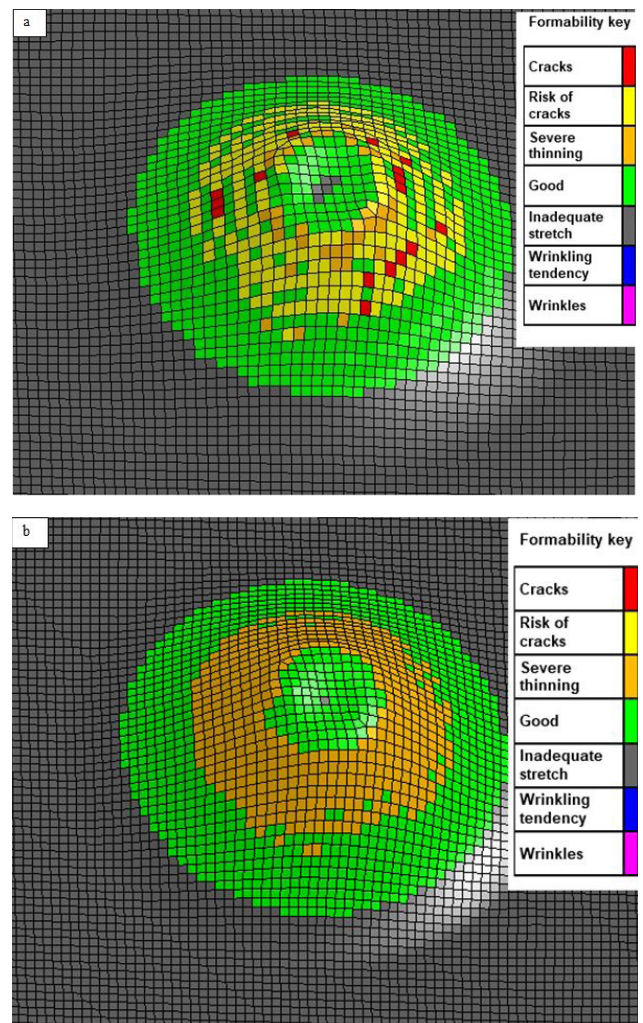

Fig. 5 Predicted formability limit with varying tool diameters ((a) 8 mm, and (b) 16 mm)
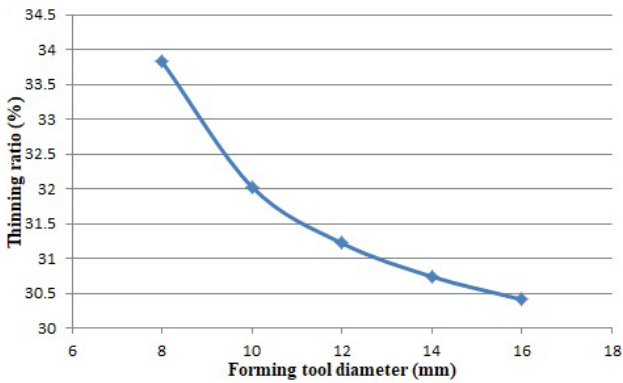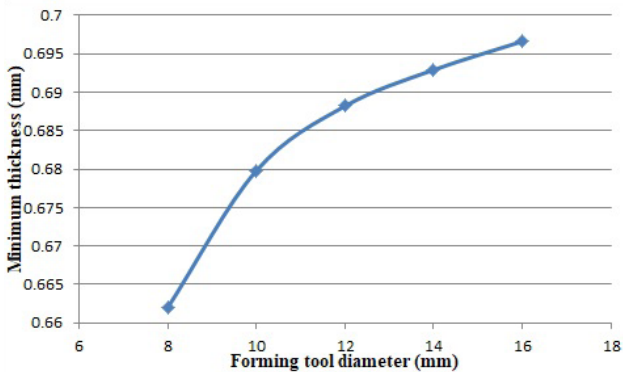

Fig. 4 Impact of tool diameter on the forming force

Fig. 6 Variation in the minimum thickness and thinning ratio with respect to tool diameter
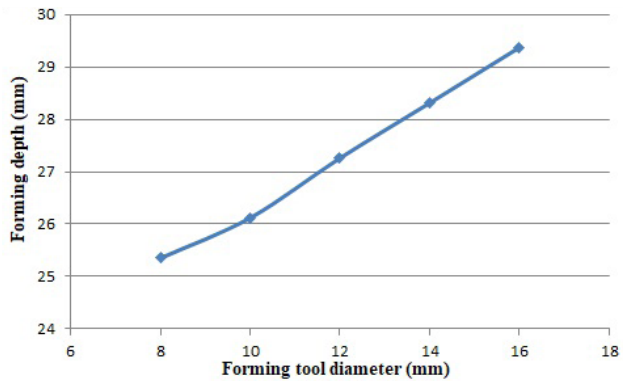

Fig. 7 Correlation between tool diameter and forming depth

a larger incremental forming tool diameter, which are in good agreement with [31, 32].

The predicated effective plastic strain with varying tool diameters shows that the effective plastic strain decreased with the increase in tool diameter. This phenomenon might be attributed to the increasing contact area and deformation zone (Fig. 8), which is consistent with the finding in [29].

According to the above observations, a larger tool diameter (16 mm) reveals better results compared with a smaller tool diameter (8 mm). Therefore, the larger tool diameter was used to conduct the later experiments of the SPIF process of the AA1050 aluminium alloy and DC04 carbon steel.
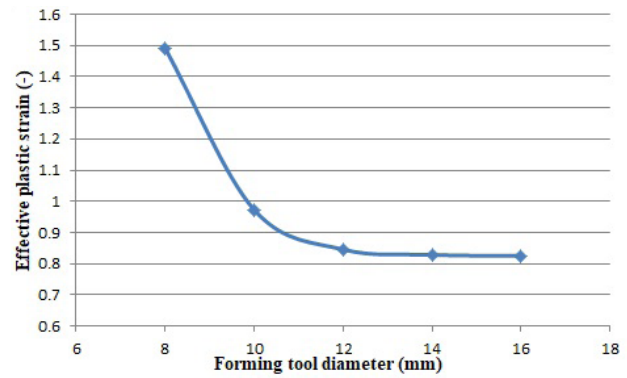

Fig. 8 Influence of forming tool diameter on the effective plastic strain

4.2 Forming force

Various wall angles were used to form the sheet metals to identify the maximum forming angle that the sheet metal reaches without failure. The results indicate that AA1050 aluminium alloy can be formed up to 72° without failure. By contrast, the maximum forming angle of DC04 carbon steel without fracture was recorded at 75°. Fig. 9 shows the findings of the FEM experiments on the influence of different forming angles (45°, 55°, 65°, 70°, 72°, 75° and 80°) on the resultant forming force of AA1050 aluminium alloy and DC04 carbon steel. The forming force observations indicate that the forming force was raised with the increase in the wall angle because the sheet metal is deformed and strained more for each pass, requiring more
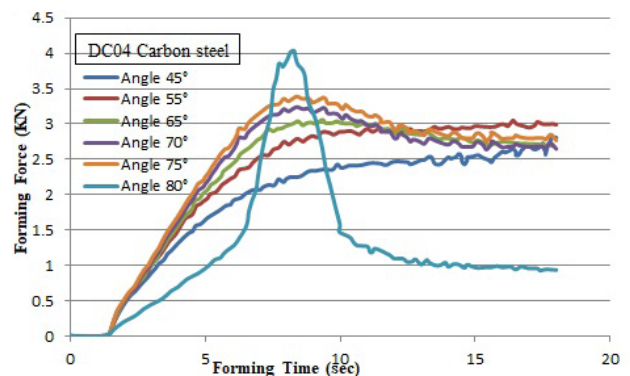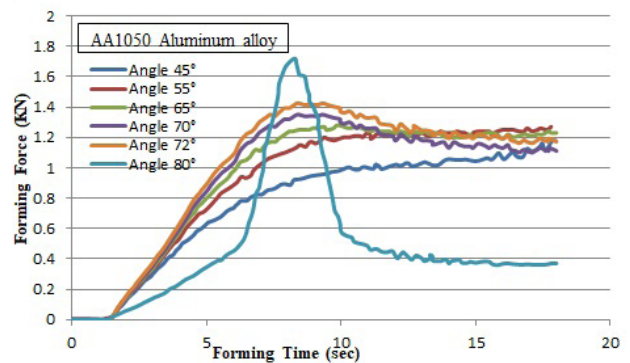

Fig. 9 Resultant forming force with varying wall angles

energy input to form the blank sheet, more surface area of spherical tool tip will be in contact with the specimen. Therefore, the contact region between the sheet and the tool interface is more for local deformation due to the rise in the required forming forces, which is consistent with the results in [11–13].

Another interesting point has been observed for the forming angle below 55°. The forming force gradually increased until it reached the peak force and continue to slowly increase until the end of the experiment. Meanwhile, the forming force of the wall angles greater than 55° to 75° progressively increases until it reaches its maximum value. Thereafter, the curve slightly decreased and later settled at a specific value, remaining at this level of force value until the process was completed. The curve of the 80° angle increases until it reaches the peak force, then descends to a specific point and remains at this point until the process is completed. Furthermore, three different types of forming force were observed after reaching the peak values for both sheet metals used in this work. The first one is a steady-state trend, which is observed for the wall angles less than 55°, the second one is a polynomial for wall angles 65° to 75°, while the third one is a monotonic reduction for wall angles greater than 80°, as shown in Fig. 8. This phenomenon occurs because the blank sheet experiences a longer bending effect before strain hardening when the smaller forming angles are below 55°. After the forming force reached the peak value, it becomes a steady-state trend, and the force increased after the maximum value is reached due to the generation of strain hardening in the sheet metal. By contrast, the reduction is due to the thinning. Consequently, strain hardening is critical for smaller wall angles to compensate for the sheet metal thinning, and the force remains steady avoiding the occurrence of fracture and the successfully formed parts at this stage.

A polynomial trend was noticed after the peak value for angles 65° to 75° is reached, which is attributed to the impact of thinning at the beginning of stretching, resulting in the slight decline in force. After this point, the forming force becomes steady until the operation is completed. The formed components with this trend have been produced without any indication of failure. A monotonic decrease has been observed in wall angles greater than 80°. This notion means that strain hardening will not be able to recompense the impact of sheet thinning, resulting in the inhomogeneous behaviour of the operation and rapid decline in the forming forces, indicating the failure

of the sheet metal, and some materials have been removed, which are match with the results in [13]. The results also reveal that the forming forces required to deform the DC04 carbon steel are more than those of AA1050 aluminium alloy resulting from the high values of strain hardening (n) and the strength coefficient (K) of DC04. Higher values of K and n result in more strengthening in the wall of formed parts, which requires more energy input and forming force to deform the sheet metal.

4.3 Wall thickness

In this study, the experimental measurement of thickness variation and the thinning ratio of the successfully formed parts along the inclined wall of the product of both sheet metals was performed by cutting the final specimen into equal half parts and determining the thickness distribution with the aid of a micrometre at five different locations along the sidewall, as shown in Fig. 10.

Variation in thickness distribution and thinning ratio of AA1050 aluminium alloy and DC04 carbon steel are quite prominent and critical due to the increase of the forming angle. Therefore, the influence of forming angles was used to determine their impact on the thickness variation and thinning ratio in the experimental and simulation results, as shown in Fig. 11 and Fig. 12.

These figures demonstrate there are three distinguished regions along with the wall profile. The first region near the clamping plate exhibits with a bent shape and a slightly reduced thickness profile. The middle region is regarded as the thinnest area with a cone profile where the maximum straining occurs, and it is disturbed by the thinning impact. These results are generated due to the hoop strain in this region. Besides the deformation, longitudinal strains occur due to the hoop strains despite the value of forming angles. Another interesting observation is that the

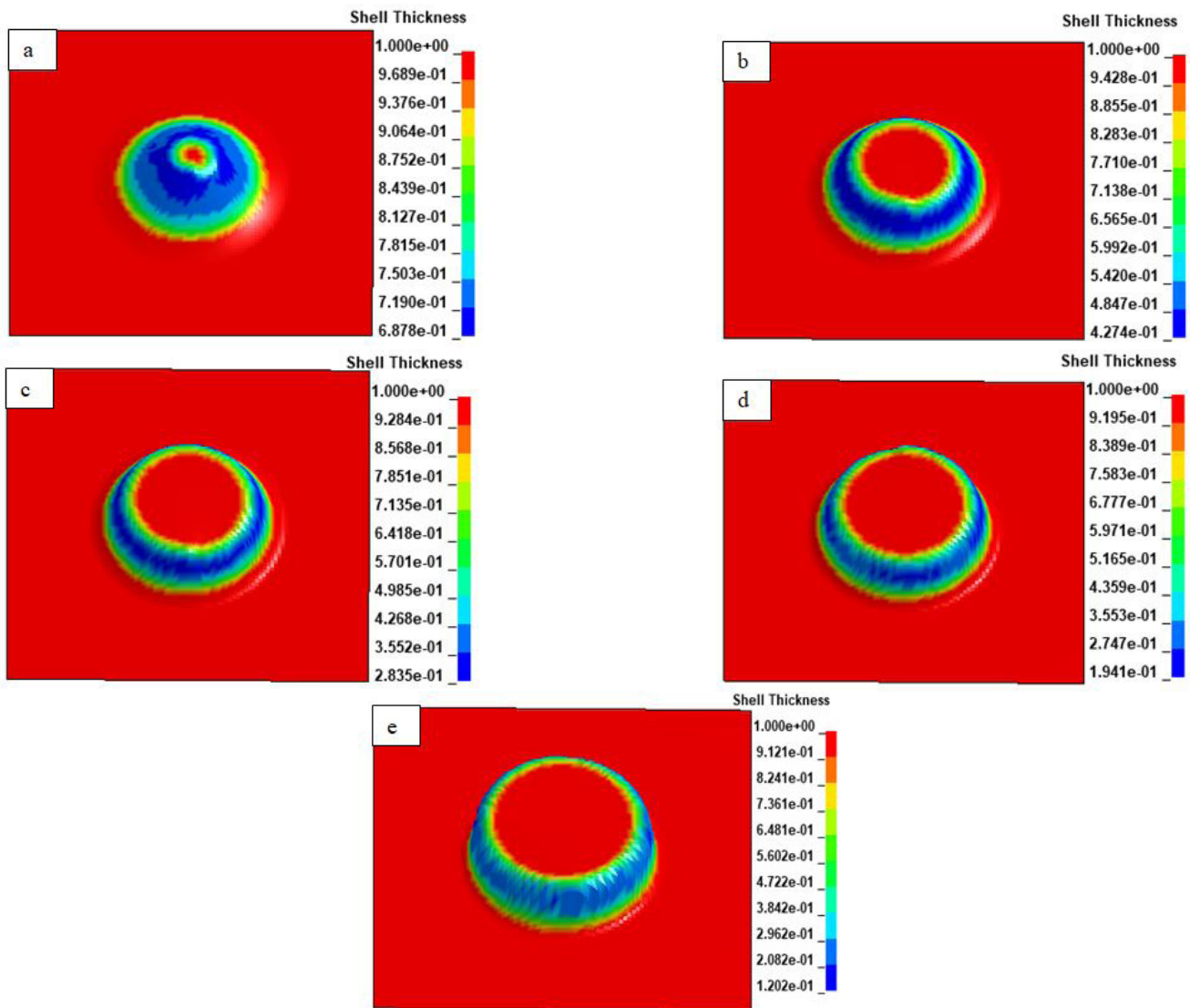**Fig. 10** Method of the measurement of thickness distribution

Fig. 11 Numerical simulation results of the thickness variation of AA1050 at different forming angles ((a) 55°, (b) 60°, (c) 65°, (d) 70° and (e) 72°)

relationship between the effective plastic strain and the wall angle is proportional, which means that the plastic strain increases with the rise in the forming angle, as shown in Fig. 13. Additionally, the observation of the effective plastic strain was axisymmetric of the formed cone, and the effective plastic strain was observed at almost zero in the bottom region of the formed components and the flange region (the region is in contact with the clamping plate), as shown in Fig. 14, which are consistent with the results in [20]. Furthermore, the inner surface of the truncated cone experienced a more effective plastic strain compared with the outer surface because the internal part of the blank has a direct contact with the incremental forming tool. The impact of the anisotropic properties of AA1050 and DC04 sheet metals was pronounced throughout the inequality of effective plastic strain between the outer and the interior parts of the formed cone.

The results indicate a slight difference in the effective plastic strain in the transition region between the bottom corner radius and the inclined wall of the formed components, making this zone the source of crack initiation and failure. A crack opening mode (failure mode 1) was observed in the corner radius of the bottom part of the truncated cone. This mode occurred when forming a sheet metal at a forming angle equal to 80°, as shown in Fig. 15. The deformation mechanism related to fracture mode 1 occurred due to the stretching mechanism caused by meridional tensile stresses. This finding is consistent with observations in [20, 45], and the experimental results fairly correspond with the simulation outcomes. The achieved deformation in the SPIF process is more than in the traditional metal forming operations due to the hydrostatic pressure existence, which arises from the elastic deformation of the region that is adjacent to the contact area.
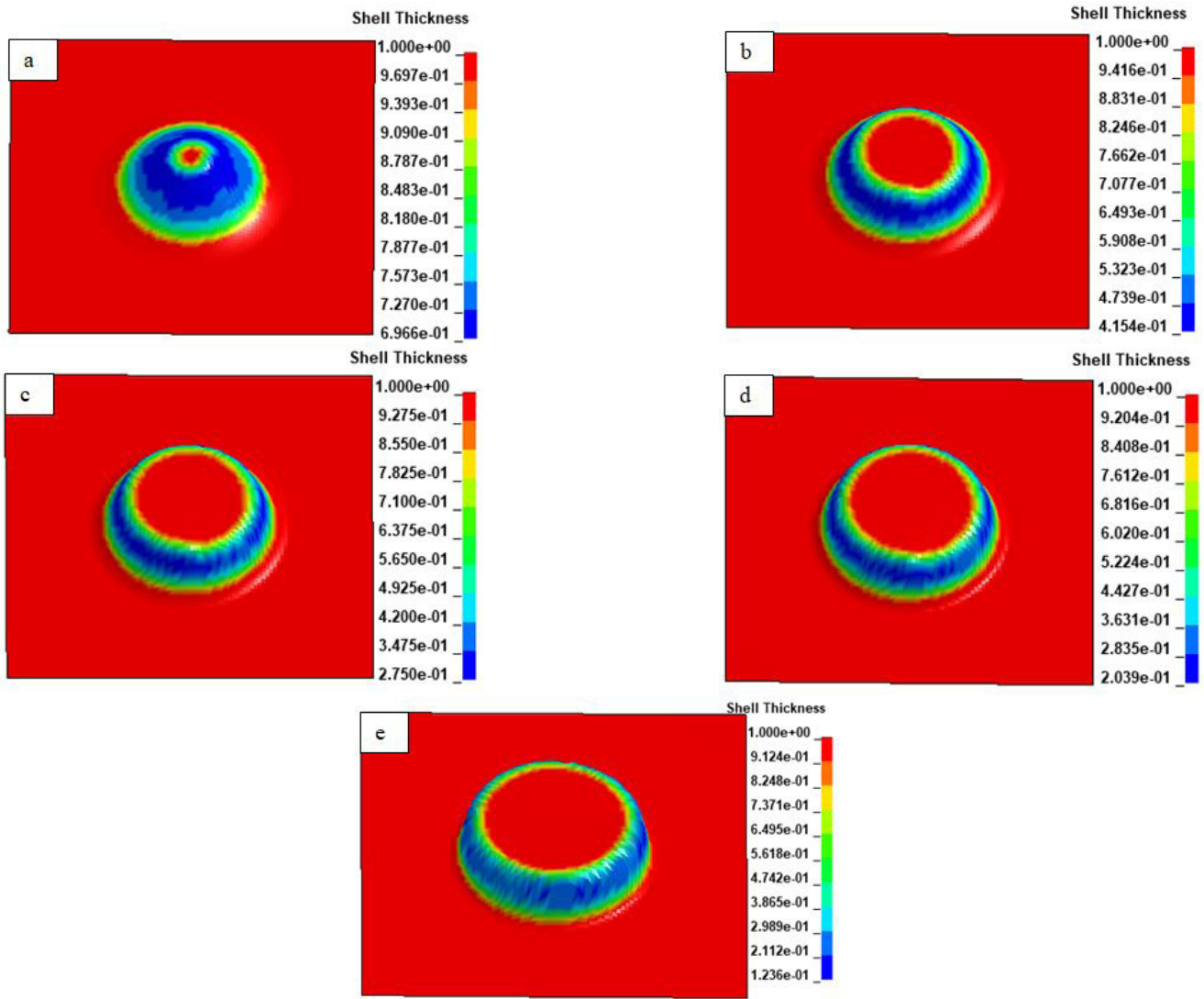
Fig. 12 Numerical simulation results of the thickness variation of DC04 at different forming angles ((a) 55°, (b) 60°, (c) 65°, (d) 70° and (e) 75°)
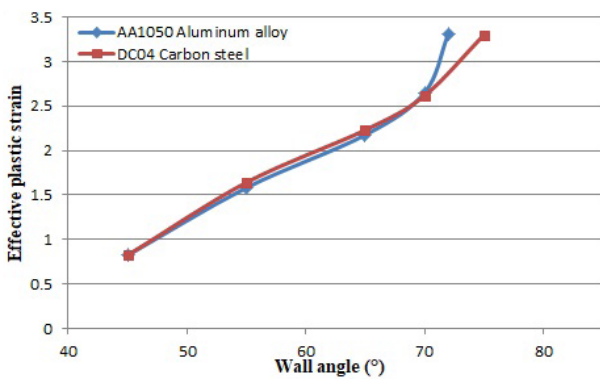

Fig. 13 Correlation between the effective plastic strain and the wall angle
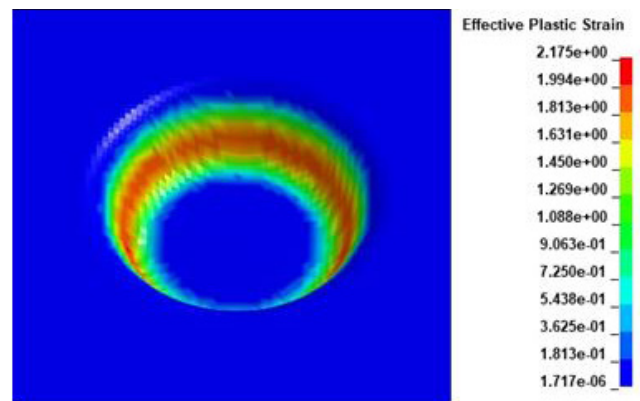

Fig. 14 Resultant of the effective plastic strain of a sample

The bottom and upper contours of the truncated cone are still unchanged and unprocessed, indicating that the variation in thickness does not influence those regions, and the final sheet thickness remains the same value as the initial thickness. The forming tool moves along the prescribed path to plastically deform the sheet material in the SPIF process. Furthermore, when the moving tool is active and touches the blank sheet surface, accumulated
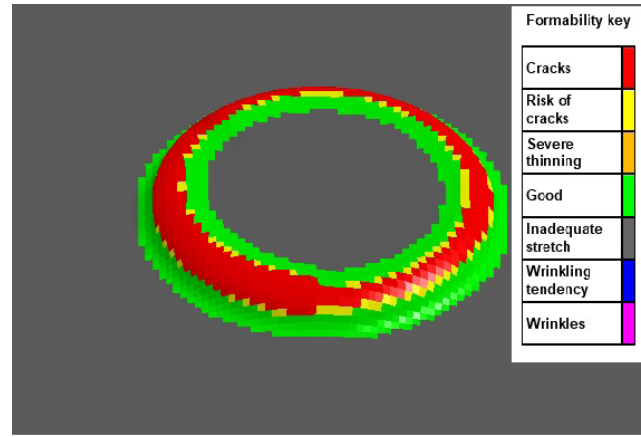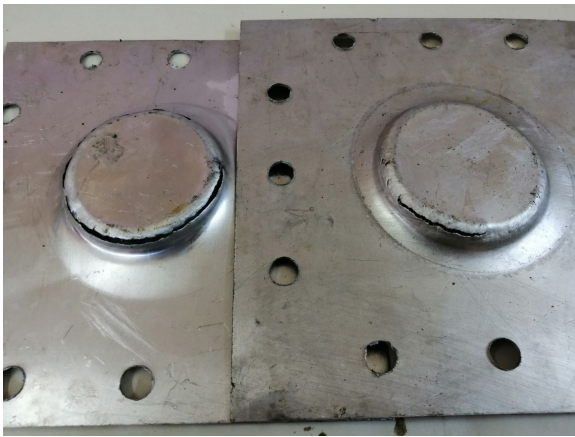
Fig. 15 Type of observed failure mode of the truncated cone at 80° angle

deformation is produced owing to the contact between the tooltip and the blank material. Even though the upper and bottom contours have no contact with the moving tool, consequently, they show the same initial thickness.

Fig. 16 and Fig. 17 show the comparison between the experimental and the numerical results of the thickness distribution of the formed components of the two sheet metals at different contact regions with respect to the
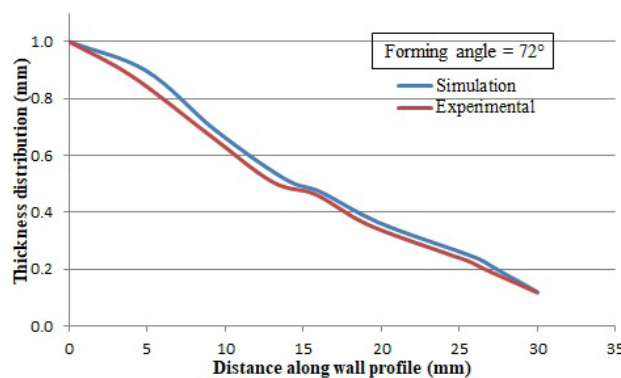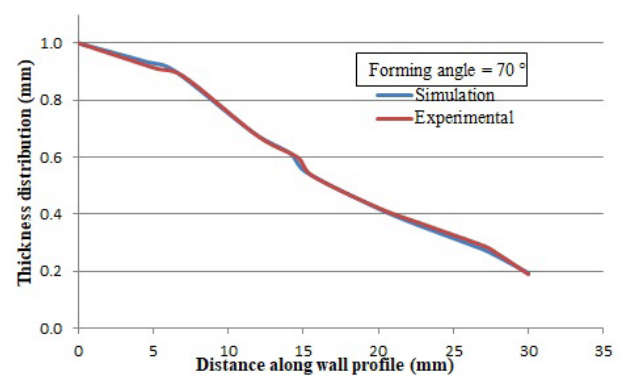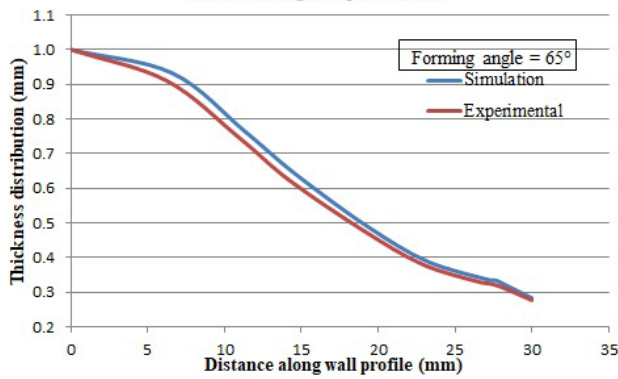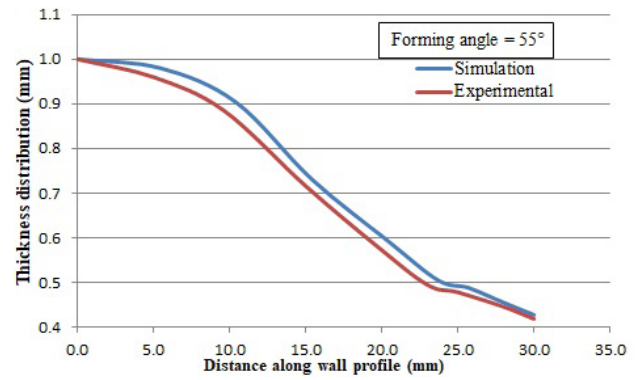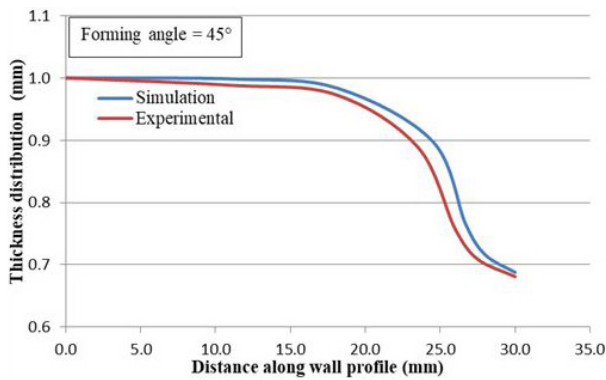

Fig. 16 FE simulation and experimental results of the thickness distribution of AA1050 aluminium alloy at different forming angles
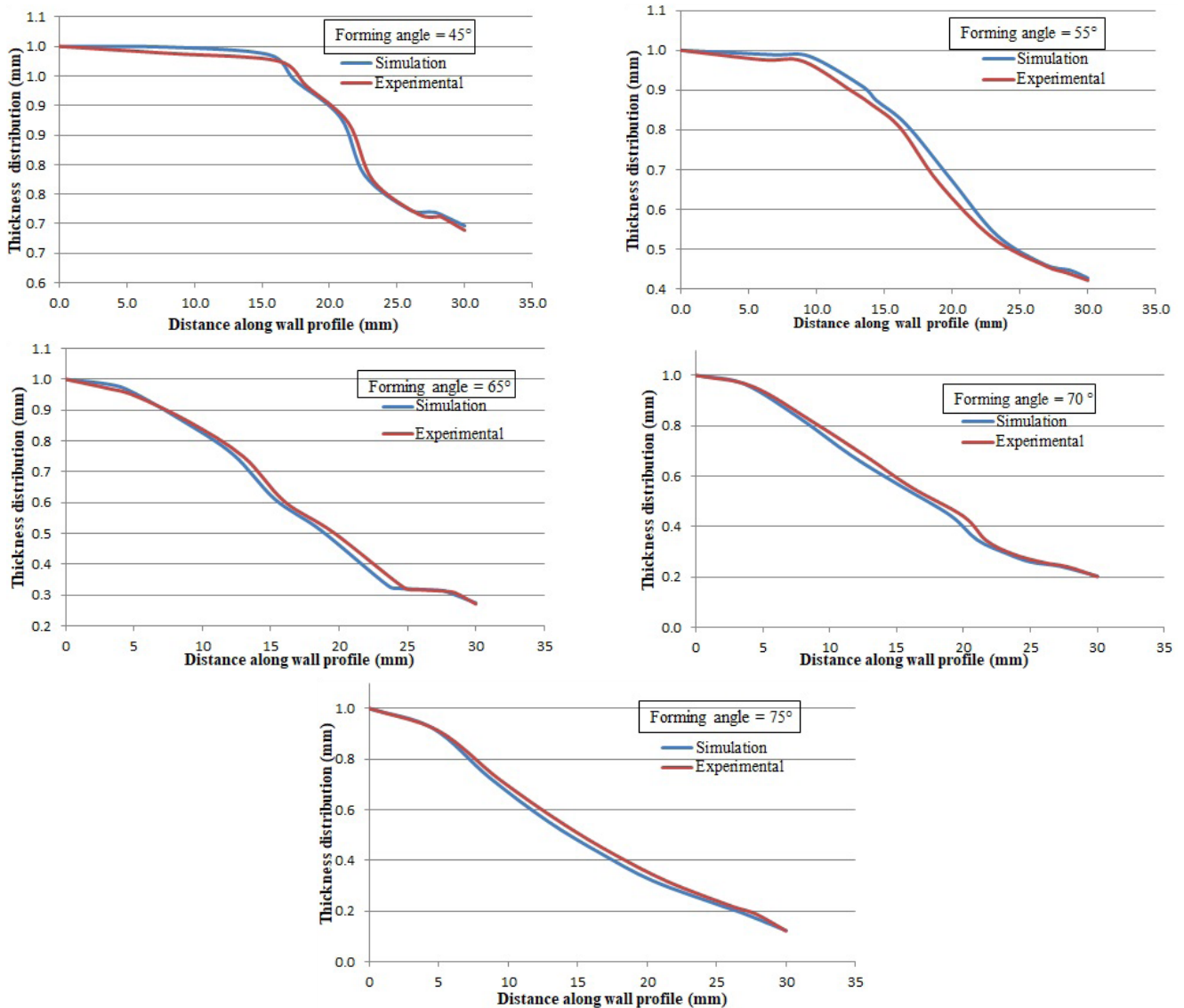
Fig. 17 FE simulation and experimental results of the thickness distribution of DC04 carbon steel at different forming angles

change of wall angle. The most remarkable point is that an irregular distribution of thickness was observed along the inclined wall for all various forming angles, and the thinning ratio was higher when the degree of wall angle increased. The formed part was particularly thin in the middle region of deformation. The thinning ratios of the samples produced at angles 45° and 55° were safe and equal to 30.41% and 58.47%, respectively. Meanwhile, the thinning ratio of the specimens within 65°, 70° and 75° were critical and equal to 72.5%, 79.61% and 87.64%, respectively. Two observations were noticed in this section. First, the inclination angle of the cone product has a vital influence on the sheet material behaviour, which is characterised by the percentage of thinning, and the obtained findings of this response is roughly at 45° twice times bigger compared with the 65° wall angle. The results observed

in both sheet metals used in this investigation agree with findings in [20, 27, 28]. Secondly, the behaviour of thickness distribution is non-homogenous and irregular along with the wall profile, which is one of the drawbacks of the SPIF process. Therefore, this factor should be taken into account when determining the maximum allowable stress and pressure that might be applied to the sheet material to prevent initiation of cracks and later occurrence of failure.

5 Conclusion

In this study, a truncated cone from AA1050 and DC04 sheet metals was formed by using the SPIF process, and the results were analysed by means of experimental and numerical investigation. The main conclusions are as follows:

- The forming force, formability and minimum thickness were increased with increasing forming tool diameter.

- The effective plastic strain of the formed components has an inverse relationship with the forming tool diameter.
- The effective plastic strain has a direct relationship with the forming angle, and it is raised by increasing the forming angle of the truncated cone.
- The forming force has been analysed based on FEM simulation. The result showed that the forming force increases with the expansion in the wall angle. Consequently, the forming force show three interesting trends with the increasing forming angle, such as steady-state, polynomial and monotonic trend. DC04 shows a higher forming force compared with AA1050 at the same parameters.
- Based on the experimental and numerical results, the homogeneity of thickness distribution along the wall profile is good and safe for forming angles less than 55°.
- The influence of forming angle on the thinning ratio and minimum thickness was investigated.

The mechanism was found from the analysis of the results. The thinning ratio rapidly increases when the wall angle increases, and the minimum thickness significantly decreases with the increase in the forming angle.

- The circumferential crack type was observed in the corner radius of the bottom part of the truncated cone.
- The DC04 carbon steel at different wall angles exhibits roughly good results compared with AA1050 aluminium alloy.
- The simulation results reveal that the Cowper Symonds criterion is well-accepted to establish the SPIF finite element model, and the experimental findings were match fairly with the simulation ones.

Acknowledgement

References

[1] Yuan, L., Ding, S., Wen, C. "Additive manufacturing technology for porous metal implant applications and triple minimal surface structures: A review", Bioactive Materials, 4, pp. 56–70, 2019.
https://doi.org/10.1016/j.bioactmat.2018.12.003

[2] Paniti, I., Viharos, Z. J., Harangozo D., Najm, S. M. "Experimental and numerical investigation of the single-point incremental forming of aluminium alloy foils", ACTA IMEKO, 9(1), pp. 25–31, 2020.
https://doi.org/10.21014/acta_imeko.v9i1.750

[3] Kumar, A., Gulati. V., Kumar, P., Singh, V., Kumar, B., Singh, H. "Parametric effects on formability of AA2024-O aluminum alloy sheets in single point incremental forming", Journal of Materials Research and Technology, 8(1), pp. 1461–1469, 2019.
https://doi.org/10.1016/j.jmrt.2018.11.001

[4] Trzepiecinski, T., Najm, S. M., Oleksik, V., Vasilca, D., Paniti, I., Szpunar, M. "Recent Developments and Future Challenges in Incremental Sheet Forming of Aluminium and Aluminium Alloy Sheets", Metals, 12(1), Article number: 124, 2022.
https://doi.org/10.3390/met12010124

[5] Duflou, J. R., Habraken, A.-M., Cao, J., Malhotra, R., Bambach, M., Adams, D., Vanhove, H., Mohammadi, A., Jeswiet, J. "Single point incremental forming: state-of-the-art and prospects", International Journal of Material Forming, 11(6), pp. 743–773, 2018.
https://doi.org/10.1007/s12289-017-1387-y

[6] Kurra, S., Rahman, N. H., Regalla, S. P., Gupta, A. K. "Modeling and optimization of surface roughness in single point incremental forming process", Journal of Materials Research and Technology, 4(3), pp. 304–313, 2015.
https://doi.org/10.1016/j.jmrt.2015.01.003

[7] Bagudanch, I., Centeno, G., Vallellano, C., Garcia-Romeu, M. L. "Forming force in Single Point Incremental Forming under different bending conditions", Procedia Engineering, 63, pp. 354–360, 2013.
https://doi.org/10.1016/j.proeng.2013.08.207

[8] Aerens, R., Eyckens, P., Van Bael, A., Duflou, J. R. "Force prediction for single point incremental forming deduced from experimental and FEM observations", The International Journal of Advanced Manufacturing Technology, 46(9), pp. 969–982, 2010.
https://doi.org/10.1007/s00170-009-2160-2

[9] Duflou, J., Tunckol, Y., Szekeres, A., Vanherck, P. "Experimental study on force measurements for single point incremental forming", Journal of Materials Processing Technology, 189(1–3), pp. 65–72, 2007.
https://doi.org/10.1016/j.jmatprotec.2007.01.005

[10] Duflou, J. R., Szekeres, A., Vanherck, P. "Force Measurements for Single Point Incremental Forming: An Experimental Study", Advanced Materials Research, 6–8, pp. 441–448, 2005.
https://doi.org/10.4028/www.scientific.net/AMR.6-8.441

[11] Filice, L., Ambrogio, G., Micari, F. "On-Line Control of Single Point Incremental Forming Operations through Punch Force Monitoring", CIRP Annals, 55(1), pp. 245–248, 2006.
https://doi.org/10.1016/S0007-8506(07)60408-9

[12] Kumar, A., Gulati, V., Kumar, P. "Investigation of Process Variables on Forming Forces in Incremental Sheet Forming", International Journal of Engineering and Technology, 10(3), pp. 680–684, 2018.
https://doi.org/10.21817/ijet/2018/v10i3/181003021

[13] Kumar, A., Gulati, V. "Experimental investigations and optimization of forming force in incremental sheet forming", Sādhanā, 43(10), Article number: 159, 2018.
https://doi.org/10.1007/s12046-018-0926-7

[14] Pohlak, M., Majak, J., Küttner, R. "Manufacturability and limitations in incremental sheet forming", Proceedings of the Estonian Academy of Sciences, 13(2), pp. 129–139, 2007.

[15] Li, Y., Daniel, W. J. T., Meehan, P. A. "Deformation analysis in single-point incremental forming through finite element simulation", The International Journal of Advanced Manufacturing Technology, 88(1), pp. 255–267, 2017.
https://doi.org/10.1007/s00170-016-8727-9

[16] Li, Y., Liu, Z., Lu, H., Daniel, W. J. T., Liu, S., Meehan, P. A. "Efficient force prediction for incremental sheet forming and experimental validation", The International Journal of Advanced Manufacturing Technology, 73(1), pp. 571–587, 2014.
https://doi.org/10.1007/s00170-014-5665-2

[17] Li, Y., Daniel, W. J. T., Liu, Z., Lu, H., Meehan, P. A. "Deformation mechanics and efficient force prediction in single point incremental forming", Journal of Materials Processing Technology, 221, pp. 100–111, 2015.
https://doi.org/10.1016/j.jmatprotec.2015.02.009

[18] Fiorentino, A. "Force-based failure criterion in incremental sheet forming", The International Journal of Advanced Manufacturing Technology, 68(1), pp. 557–563, 2013.
https://doi.org/10.1007/s00170-013-4777-4

[19] Lu, B., Fang, Y., Xu, D. K., Chen, J., Ou, H., Moser, N. H., Cao, J. "Mechanism investigation of friction-related effects in single point incremental forming using a developed oblique roller-ball tool", International Journal of Machine Tools and Manufacture, 85, pp. 14–29, 2014.
https://doi.org/10.1016/j.ijmachtools.2014.04.007

[20] Neto, D. M., Martins, J. M. P., Oliveira, M. C., Menezes, L. F., Alves, J. L. "Evaluation of strain and stress states in the single point incremental forming process", The International Journal of Advanced Manufacturing Technology, 85(1), pp. 521–534, 2016.
https://doi.org/10.1007/s00170-015-7954-9

[21] Emmens, W. C., van der Weijde, D. H., van den Boogaard, A. H. "The FLC, enhanced formability, and incremental sheet forming", In: International Deep Drawing Research Group IDDRG 2009 International Conference, Golden, CO, USA, 2009, pp. 773–784.

[22] Jackson, K., Allwood, J. "The mechanics of incremental sheet forming", Journal of Materials Processing Technology, 209(3), pp. 1158–1174, 2009.
https://doi.org/10.1016/j.jmatprotec.2008.03.025

[23] Ambrogio, G., Filice, L., Micari, F. "A force measuring based strategy for failure prevention in incremental forming", Journal of Materials Processing Technology, 177(1–3), pp. 413–416, 2006.
https://doi.org/10.1016/j.jmatprotec.2006.04.076

[24] Oraon, M., Sharma, V. "Prediction of surface roughness in single point incremental forming of AA3003-O alloy using artificial neural network", International Journal of Materials Engineering Innovation, 9(1), pp. 1–19, 2018.
https://doi.org/10.1504/IJMATEI.2018.092181

[25] Petek, A., Kuzman, K., Kopač, J. "Deformations and forces analysis of single point incremental sheet metal forming", Archives of Materials Science and Engineering, 35(2), pp. 107–116, 2009.

[26] Blaga, A., Bologa, O., Oleksik, V., Pîrvu, B. "Experimental researches regarding the influence of geometric parameters on the principal strains and thickness reduction in single point incremental forming", UPB Scientific Bulletin, Series D, 74(2), pp. 111–120, 2012.

[27] Abdelkadera, W. B., Bahloula, R., Arfaa, H. "Numerical Investigation of the Influence of some Parameters in SPIF Process on the Forming Forces and Thickness Distributions of a Bimetallic Sheet CP-Titanium/Low-carbon Steel Compared to an Individual Layer", Procedia Manufacturing, 47, pp. 1319–1327, 2020.
https://doi.org/10.1016/j.promfg.2020.04.252

[28] Arfa, H., Abdelkader, W. B., Bahloul, R. "Numerical study of SPIF process of Al-Cu bimetal sheet using finite element analysis: Influence of process parameters on the mechanical and geometrical responses", In: Aifaoui, N., Affi, Z., Abbes, M. S., Walha, L., Haddar, M., Romdhane, L., Benamara, A., Chouchane, M., Chaari, F. (eds.) Design and Modeling of Mechanical Systems - IV, Springer, Cham, Switzerland, 2020, pp. 487–497.
https://doi.org/10.1007/978-3-030-27146-6_53

[29] Mezher, M. T., Namer, N. S. M., Nama, S. A. "Numerical and experimental investigation of using lubricant with nano powder additives in SPIF process", International Journal of Mechanical Engineering and Technology, 9(13), pp. 968–977, 2018.

[30] Namer, N. S. M., Naáma, S. A., Mazhir, M. T. "Influence of lubricant viscosity on the surface roughness of PEHD and PVC plastic sheets in single point incremental forming process", International Journal of Engineering and Applied Sciences, 7(2), pp. 27–30, 2015.

[31] Li, Y., Liu, Z., Daniel, W. J. T., Meehan, P. A. "Simulation and Experimental Observations of Effect of Different Contact Interfaces on the Incremental Sheet Forming Process", Materials and Manufacturing Processes, 29(2), pp. 121–128, 2014.
https://doi.org/10.1080/10426914.2013.822977

[32] Golabi, S., Khazaali, H. "Determining frustum depth of 304 stainless steel plates with various diameters and thicknesses by incremental forming", Journal of Mechanical Science and Technology, 28(8), pp. 3273–3278, 2014.
https://doi.org/10.1007/s12206-014-0738-6

[33] Mezher, M. T., Khazaal, S. M., Namer, N. S. M., Shakir, R. A. "A comparative analysis study of hole flanging by incremental sheet forming process of AA1060 and DC01 sheet metals", Journal of Engineering Science and Technology, 16(6), pp. 4383–4403, 2021.

[34] Najm, S. M., Paniti, I. "Study on Effecting Parameters of Flat and Hemspherical end Tools in SPIF of Aluminium Foils", Tehnički Vjesnik, 27(6), pp. 1844–1849, 2020.
https://doi.org/10.17559/TV-20190513181910

[35] Najm, S. M., Paniti, I. "Experimental Investigation on the Single Point Incremental Forming of AlMn1Mg1 Foils using Flat End Tools", IOP Conference Series: Material Science and Engineering, 448, Article number: 012032, 2018.
https://doi.org/10.1088/1757-899X/448/1/012032

[36] Najm, S. M., Paniti, I., Trzepieciński, T., Nama, S. A., Viharos, Z. J., Jacso, A. "Parametric Effects of Single Point Incremental Forming on Hardness of AA1100 Aluminium Alloy Sheets", Materials, 14(23), Article number: 7263, 2021.
https://doi.org/10.3390/ma14237263

[37] Najm, S. M., Paniti, I., Viharos, Z. J. "Lubricants and Affecting Parameters on Hardness in SPIF of AA1100 Aluminium", In: 17th IMEKO TC 10 and EUROLAB Virtual Conference: "Global Trends in Testing, Diagnostics & Inspection for 2030", Dubrovnic, Croatia, 2020, pp. 387–392.

[38] Najm, S. M., Paniti, I. "Artificial neural network for modeling and investigating the effects of forming tool characteristics on the accuracy and formability of thin aluminum alloy blanks when using SPIF", The International Journal of Advanced Manufactoring Technology, 114(9), pp. 2591–2615, 2021.
https://doi.org/10.1007/s00170-021-06712-4

[39] Najm, S. M., Paniti, I. "Predict the Effects of Forming Tool Characteristics on Surface Roughness of Aluminum Foil Components Formed by SPIF Using ANN and SVR", International Journal of Precision Engineering and Manufacturing, 22(1), pp. 13–26, 2021.
https://doi.org/10.1007/s12541-020-00434-5

[40] Namer, N. S. M., Nama, S. A., Mezher, M. T. "The influence of Nano particles additive on tribological properties of AA2024-T4 coated with TiN or SiN thin films", Journal of Mechanical Engineering Research and Developments (JMERD), 42(3), pp. 30–34, 2019.

[41] ASTM International "ASTM E8/E8M-21, Standard Test Methods for Tension Testing of Metallic Materials", ASTM International, West Conshohocken, PA, USA, 2004.
https://doi.org/10.1520/E0008_E0008M-21

[42] Pohlak, M., Küttner, R., Majak, J., Karjust, K., Sutt, A. "Simulation of incremental forming of sheet metal products", In: Papstel, J., Katalinic, B. (eds.) Proceedings of the 4th International DAAAM Conference "Industrial Engineering - Innovation as Competitive Edge for SME", Tallinn, Estonia, 2004, pp. 143–145.

[43] Mezher, M. T., Saad, M. L., Barrak O. S., Shakir, R. A. "Finite Element Simulation and Experimental Analysis of Nano Powder Additives Effect in the Deep Drawing Process", International Journal of Mechanical and Mechatronics Engineering IJMME-IJENS, 20(1), pp. 166–180, 2020.

[44] Mezher, M. T., Barrak, O. S., Nama, S. A., Shakir, R. A. "Predication of Forming Limit Diagram and Spring-back during SPIF process of AA1050 and DC04 Sheet Metals", Journal of Mechanical Engineering Research and Developments, 44(1), pp. 337–345, 2021.

[45] Silva, M. B., Skjoedt, M., Martins, P. A. F., Bay, N. "Revisiting the fundamentals of single point incremental forming by means of membrane analysis", International Journal of Machine Tools and Manufacture, 48(1), pp. 73–83, 2008.
https://doi.org/10.1016/j.ijmachtools.2007.07.004